ACS APPLIED POLYMER MATERIALS

pubs.acs.org/acsapm Article

Multifunctional Gas-Spinning Hierarchical Architecture: A Robust and Efficient Nanofiber Membrane for Simultaneous Air and Water Contaminant Remediation

Dan Lv, Guosheng Tang, Long Chen, Mengjie Zhang, Jiaxin Cui, Ranhua Xiong,* and Chaobo Huang*

Cite This: *ACS Appl. Polym. Mater.* 2020, 2, 5686−5697 Read Online

ACCESS | Metrics & More | Article Recommendations | Supporting Information

ABSTRACT: Today, poor water and air quality caused by fine particulate matters (PMs), toxic spills, and antibiotic-containing wastewater are posing serious threats and risks to the environment and human health. Although many contaminant materials can be effectively removed by the traditional membrane technology, the simultaneous multifunctional materials like PM removal, oily water separation, and antibiotic adsorption are rarely reported. In addition, most of the membranes are destroyed when working in the harsh environment such as high temperatures, high pressures, strong acids and bases, and so on. In this work, a multifunctional Fe_3O_4@polyacrylonitrile/chitosan (Fe_3O_4@PAN/CS) membrane with robust stability and repeatable usage was fabricated via a simple and environment-friendly gas-spinning method; the obtained functional membrane is supposed to be applied in both air and liquid contaminant remediation. In comparison with the reported membranes, the multifunctional Fe_3O_4@PAN/CS composite nanofiber membranes not only have excellent performance in air filtration, antibiotic adsorption, or oil−water separation but also show robust reusability and durability even in harsh environments. Our strategy would bring ideas to the design and fabrication of multifunctional membranes for simultaneous environmental remediation such as air purification and wastewater treatment.

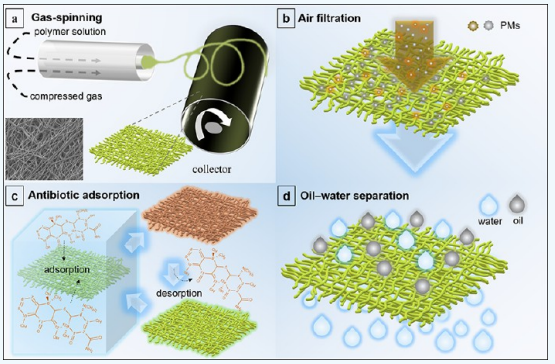

KEYWORDS: *gas-spinning, multifunctional, hierarchical architecture, contaminant remediation, nanofiber membrane*

Downloaded via HARVARD UNIV on July 24, 2021 at 14:53:49 (UTC).
See https://pubs.acs.org/sharingguidelines for options on how to legitimately share published articles.

1. INTRODUCTION

Untreated wastewater, especially wastewater from industrial and other establishments, contains a variety of hazardous substances, causing widespread disease and damage to ecosystems.[1] Taking the ever-increasing water pollution and its adverse effects on environment into consideration, researchers are focused on the design and manufacture of functional and environment-friendly materials for selective treatment of contaminated water.[2−4] Particulate matters, especially the ultrafine particulates like PM2.5 and PM0.1, pose serious risks and threats to both the ecosystem and human health, carrying annually one in every nine deaths.[5,6] Nanofibrous filtration materials are promising and effective to remove fine particles, while most of them usually show suboptimal filtration performance over ultrathin particulates, especially in harsh environments like high temperature, high pressure, and so on.[7] Therefore, the filtration and adsorption materials with the characterizations of being high temperature resistant, cost-effective, and highly efficient are urgently desired.

Nanofiber membranes with a unique 3D network structure and good internal connection channels are widely used in the field of environment remediation,[8] energy storage,[9] flexible sensing,[10] and so on. There are many methods for the fabrication of nanofiber membranes, including electrospinning,[11] melt blowing,[12] and centrifugal spinning.[13] Compared with these methods, the "gas-spinning" recently reported by our group is one of the most versatile and simple techniques to generate ultrathin nanofibers.[14] The working mechanism of the gas-spinning is similar to that of the solution blow spinning;[15,16] as shown in Figure S1, the inner needle pumps the precursor solution and the outer needle flows the pressurized gas. The pressurized gas is used to drive the polymer solution, on the one hand, and promote solvent evaporation, on the other, finally creating long fibers in a simpler one-step process. The continuous high-throughput production of long fibers can be realized by the gas-spinning method, without further treatment of drying, cooling, or washing. Compared to the traditional nanofiber fabrication techniques, the gas-spinning method has fewer process

Received: September 6, 2020
Accepted: November 9, 2020
Published: November 17, 2020

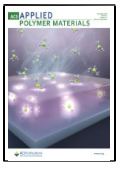

ACS Publications © 2020 American Chemical Society

https://dx.doi.org/10.1021/acsapm.0c00988
ACS Appl. Polym. Mater. 2020, 2, 5686−5697

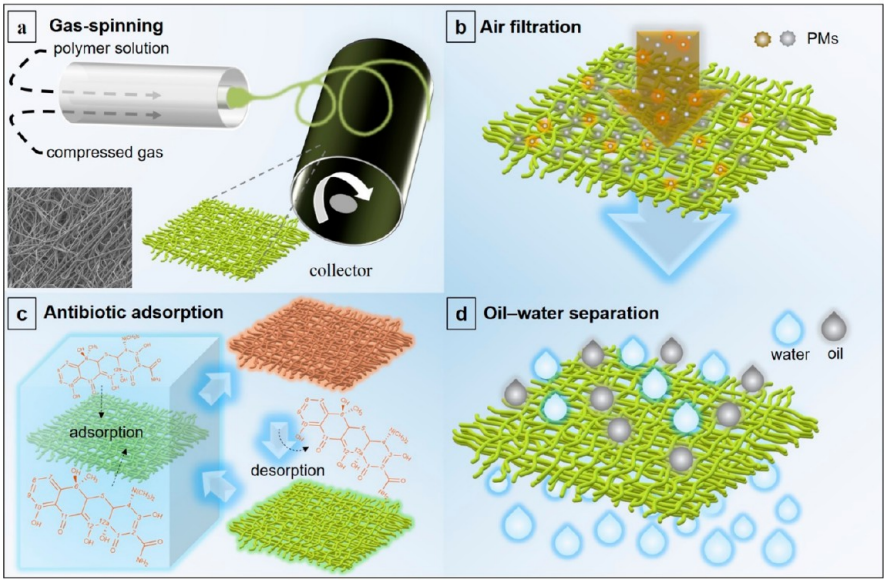

Figure 1. Multifunctional Fe_3O_4@PAN/CS composite nanofiber membranes. (a) Schematic presentation of the preparation of the membranes via gas-spinning and (b) the applications for air filtration, (c) antibiotic adsorption, and (d) oil–water separation.

requirements and avoids the high voltage and heating system. Additionally, the fiber production of the traditional technique is typically slow, while it can be simply scalable in the gas-spinning method. In a word, gas-spinning allows on-demand fiber fabrication in a simple one-step approach.

Nanofiber membranes constructed by ultrathin nanofibers are widely used in environmental remediation field including air filtration,[17] dye degradation,[18] antibiotic adsorption,[19] heavy metal ion adsorption,[20] and oily water separation.[21] However, most of the reported nanofibrous membranes mainly focused on only one of these applications and usually cannot meet the application requirements in various conditions. The new type of multifunction nanofiber membrane is highly desired. So far, there are rare reports about the multifunctional nanofiber membranes simultaneously with the characteristics of oil–water separation, antibiotic adsorption, and PM removal. Moreover, most of the multifunctional nanofibrous membranes show unsatisfactory application performance in harsh environments like high temperatures, high pressures, strong acids and bases, and so on.[22] Thus, we want to design a multifunctional architecture for simultaneous applications in both air and water remediation.

Nanofibers are excellent supports for the incorporation of nanoparticles (NPs) by virtue of the interconnected channeling pore structures.[23] The incorporation of nanoparticles and nanofibers endows the nanofiber membranes with more functions like photocatalysis, adsorption, degradation, and so on. Iron oxides have been widely studied by virtue of the geological abundance, environmentally benign, and functional properties.[24,25] Herein, we proposed a new approach to generate nanofibers in a green, low cost, simple, and scalable way. Fe_3O_4 NPs were used as the loading particles to provide more active sites for the interaction with pollutant particles and ensure robust interaction with the antibiotic. PAN was chosen as the template for the deposition of Fe_3O_4 NPs by virtue of its superhydrophilic property, gas-spinnability, and high mechanical strength, making it suitable for multiple applications. Besides, the bio-based chitosan was added to provide more functional groups to form robust interaction with pollutants. In addition, the gas-spinning nanofiber membrane loaded with Fe_3O_4 NPs shows stable superhydrophilicity and superoleophobic property in air and under water, which could be applied for the effective oil–water separation. Moreover, the multifunctional nanofiber membranes could also enable high performance in extreme environments (e.g., high temperature, high pressure, and strong acid or base). As shown in Figure 1, the as-synthesized hierarchical Fe_3O_4@PAN/CS architecture not only shows highly efficient removal of PMs in air but also possesses great potential filtration of complex contaminants in water, including oil and antibiotics.

2. MATERIALS AND METHODS

2.1. Materials. Polyacrylonitrile (PAN, M_w = 150000), chitosan (CS, M_w = 3000), and iron oxide nanoparticles (Fe_3O_4 NPs, 50 ± 20 nm) were purchased from Shanghai Macklin Biochemical Co., Ltd., China. *N*,*N*-Dimethylformamide (DMF), acetic acid, sodium hydroxide (NaOH), and hydrochloric acid (HCl) were purchased from Sinopharm Chemical Reagent Co. Ltd., China. Tetracycline hydrochloride ($C_{22}H_{24}N_2O_8$·HCl, USP) was obtained from Shanghai Aladdin Biochemical Technology Co., Ltd., China. The water system filter (0.45 μm) was purchased from Whatman Co. All chemicals were used without further purification.

2.2. Preparation of PAN Nanofibers. PAN precursor solution (12 wt %) was obtained by dissolving the PAN powder in DMF solution and continuously stirred at 60 °C for 4 h. Then the precursor solution was transferred into a 5 mL plastic syringe attached with a core–shell needle (Figure S1) and pumped out with the speed of 3 mL h^{-1}. The airflow was set to 10 L min^{-1}; the generated nanofibers (NFs) were collected by a grounded rotating metal drum, and the collecting distance was 20 cm. The collecting time was controlled to ensure the similar thickness of the nanofiber membranes. The temperature and relative humidity were controlled to 25 ± 2 °C and 40 ± 2%, respectively.

2.3. Preparation of Fe_3O_4@PAN and Fe_3O_4@PAN/CS Composite Nanofiber Membranes. Five grams of Fe_3O_4 magnetic nanoparticles was dissolved in the pre-prepared PAN solution (95 g) and stirred for 4 h, followed by the ultrasonic treatment for 2 h to form a homogeneous precursor gas-spinning solution. Then the composite solution was transferred to the gas-spinning setup to generate ultrathin nanofibers loaded with Fe_3O_4 magnetic NPs (Fe_3O_4@PAN composite nanofibers); details about the gas-spinning

https://dx.doi.org/10.1021/acsapm.0c00988
ACS Appl. Polym. Mater. 2020, 2, 5686–5697

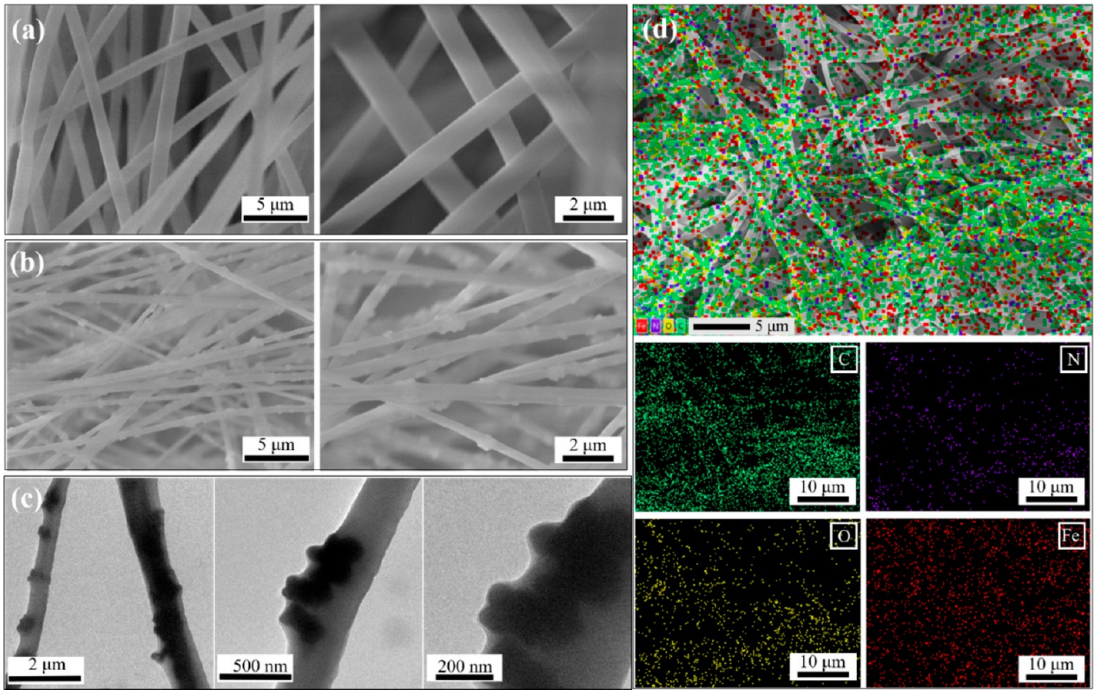

Figure 2. SEM images of (a) PAN and (b) Fe_3O_4@PAN. (c) TEM images and (d) EDS mapping of the Fe_3O_4@PAN/CS membrane.

method are provided in section 2.2. After the Fe_3O_4@PAN composite nanofiber membranes were successfully prepared, the obtained composite membranes were totally immersed in 1 wt % chitosan solution (dissolved in 1% dilute acetic acid aqueous solution) for 0.5 h and then subsequently dried (vacuum freeze-drying, −48 °C, 12 h), finally obtaining the Fe_3O_4@PAN/CS composite nanofiber membranes.

2.4. Air Filtration. The filtration performance of the Fe_3O_4@PAN/CS composite nanofiber membrane (effective area: 100 cm^2) was evaluated according to the previous published paper.[23] The filtration efficiency and pressure drop of the membrane varying in the air flow and basic weight were systematically studied. More details are provided in the Supporting Information.

2.5. Antibiotic Adsorption. The adsorption performance of the Fe_3O_4@PAN/CS composite nanofiber membranes was evaluated via the removal of tetracycline (TC), a widely used broad-spectrum antibiotic which usually causes pollution in the aquatic systems; the chemical structure is illustrated in Scheme S1. To study the adsorption properties of Fe_3O_4@PAN/CS composite membrane for TC, the adsorption performance under different conditions were tested, including the contact time, solution pH, and initial TC concentration. Then the optimum pH condition (6.00 ± 0.05) for adsorption performance was selected, and the adsorption kinetics of the adsorption process was studied. Details about the antibiotic adsorption experiment are provided in the Supporting Information.

2.6. Oil−Water Separation. The Fe_3O_4@PAN/CS composite fiber membrane was sandwiched between two custom glass tubes with a diameter of 1.5 cm. The oil−water mixture was poured into the upper glass tube, and the time of the complete separation of oil−water mixture was recorded by a stopwatch. During the oil−water separation process, the preparation membranes were tested for 50 cycles to further verify the durability and recyclability of the Fe_3O_4@PAN/CS composite nanofiber membrane. The oil water separation flow rate and separation efficiency were calculated (Supporting Information).

2.7. Characterizations. The morphologies, element compositions, and elemental distribution maps of the composite nanofiber membranes were acquired by field-emission scanning electron microscopy (FE-SEM, JSM-7600F, JEOL, Japan). TEM photographs of the samples were examined by a transmittance electron microscope (TEM, JEM-700, JEOL, Japan). The X-ray diffraction (XRD, Ultima IV, Rigaku, Japan) and X-ray photoelectron spectrometers (XPS, AXIS Ultra DLD, UK) were used to characterize the membrane. Nitrogen adsorption−desorption isotherms were conducted at 77 K (Quantachrome BET instrument, Quantachrome, USA). The thermogravimetric analyzer (TGA, Q5000-IR, TA Instruments) was used to evaluate the thermal stability of the membranes. The Fourier transform infrared spectrometer (FT-IR, Nicolet 8700, USA) was also used to determine the chemical properties. The residual Fe concentration was detected by inductively coupled plasma atomic emission spectroscopy (ICP-MS, PerkinElmer Nixon 300X). The TC concentrations were characterized by a UV−vis diffuse reflectance spectra spectrophotometer (UV-2600, Shimadzu, Japan). The mechanical strength was characterized by a universal testing machine (Sans UTM6502, China). The contact angles (CAs) were measured with a contact angle meter (JC2000D1, Zhong Chen, China).

3. RESULTS AND DISCUSSION

3.1. Fe_3O_4@PAN/CS Composite Nanofiber Membranes. The surface roughness of the membranes could be significantly enhanced by the corporation of nanoparticles in the nanofiber, which not only avails enhanced mechanical properties but also profits the filtering performance of the composite membranes.[26,27] To improve the adsorption capacity of the membrane, iron oxides nanoparticles are incorporated since it can form stable metal−ligand complexes with organic pollutes like antibiotics.[28] Taking the above points into consideration, magnetic Fe_3O_4 nanoparticles were helpful to enhance the TC adsorption performance as well as the mechanical strength when incorporated into the PAN nanofibers.

As shown in Figure 2, SEM was utilized to observe the surface morphology of the composite membranes. The long and cylindrically shaped pure PAN nanofibers with a relatively smooth surface were observed in Figure 2a, which were randomly distributed with the average diameter of 791.6 ± 92 nm (Figure S3a). The Fe_3O_4 nanoparticles tend to be encapsulated by the nanofiber since the size (50 ± 10 nm) is relatively smaller, and the original smooth nanofiber turned

https://dx.doi.org/10.1021/acsapm.0c00988
ACS Appl. Polym. Mater. 2020, 2, 5686−5697

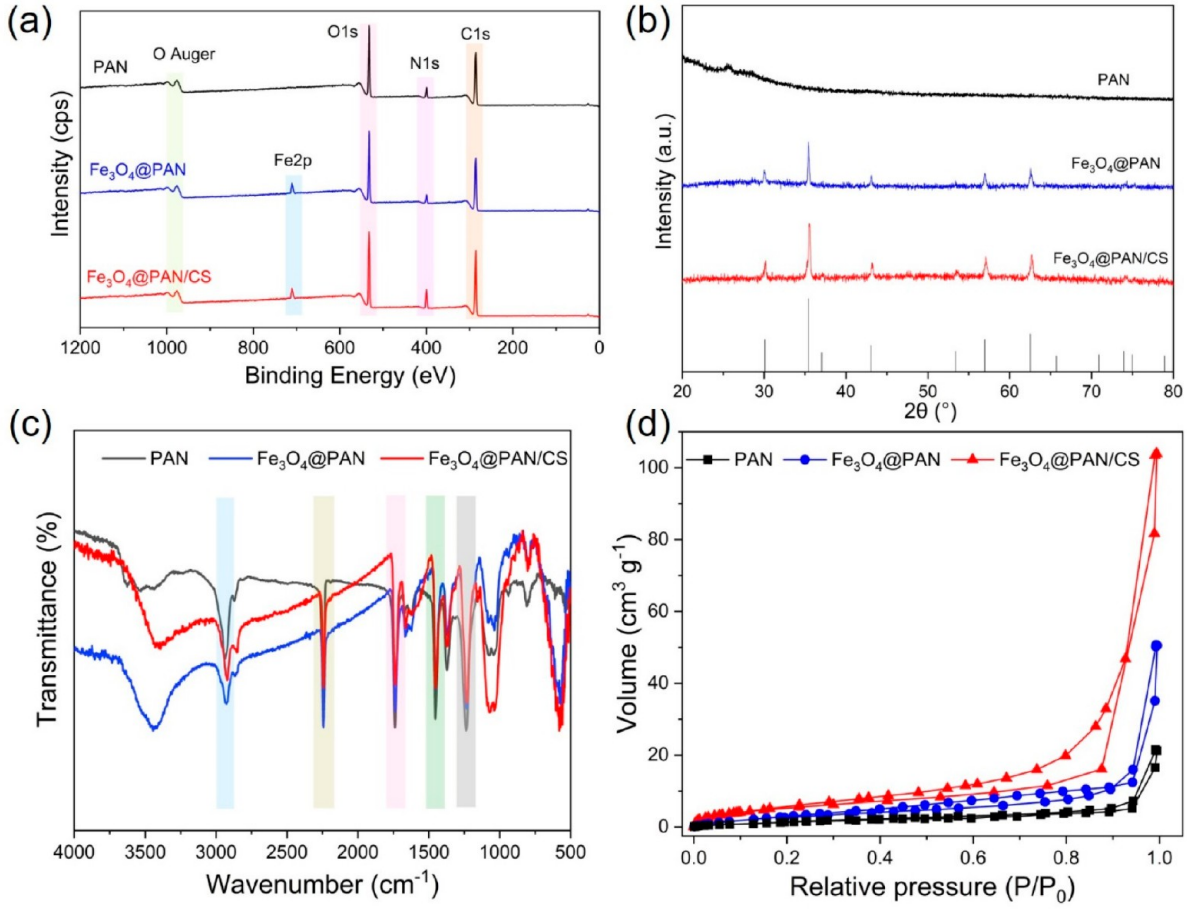

Figure 3. Characterization of the membranes: (a) XPS spectra, (b) XRD patterns, (c) FTIR spectra, and (d) N_2 adsorption/desorption isotherms of PAN, Fe_3O_4@PAN, and Fe_3O_4@PAN/CS membrane.

to be rougher with an average fiber diameter of 499.6 ± 97 nm (Figure S3b). TEM images in Figure 2c presented that the Fe_3O_4 NPs and the clusters are attached to the PAN fibers and distributed in the surface of fibers. The fibers become or cause to become stuck and glued together after the coating and modification of chitosan solution (Figure 2d), and the average diameter was 526.5 ± 92 nm (Figure S3c). Meanwhile, as shown in Figure S4, the energy-dispersive spectrometry (EDS) results confirmed that Fe_3O_4 NPs were successfully loaded in the membrane, while the N element was not detected due to the detection limit of the analyzer. Then we further utilized the X-ray photoelectron spectrometer to prove the existence of the N element; as shown in Figure 3a, the peak of N_{1s} was found at 398.4 eV.

The characterizations of the membranes are presented in Figures 3 and 4. EDS elemental mapping images demonstrated the heterogeneous structures of the composite nanofibers, which consists of the C and N elements, and a uniformed surface coating of Fe_3O_4 NPs are also found to be distributed. The peaks of Fe_3O_4 observed at 710.5 eV (Figure 3a) further proved that the Fe_3O_4 NPs were stable in oxidation. The survey XPS spectra present the chemical information about the Fe_3O_4@PAN/CS composite membrane, which agrees with the EDS results. The phase structure of the as-prepared Fe_3O_4@PAN/CS composite membranes was analyzed; as shown in Figure 3b, the diffraction peak observed at 2θ = 25.6° corresponds to the (002) plane of pure PAN.[29] The diffraction peaks of the composite membranes also match well with the Fe_3O_4 NPs, i.e., 30.1° (220), 35.4° (311), 43.1° (400), 56.9° (511), and 62.6° (440).[30] As expected, all of the diffraction peaks of the as-prepared composite membrane in the XRD pattern are matched to the standard PDF cards (JCPDS Card No. 19-0629).[31] These results further confirmed that the gas-spinning process can directly form densely hierarchical structure. In the FTIR spectrum of Fe_3O_4@PAN/CS (Figure 3c), the absorption peak at 2245 cm^{-1} is attributed to the "−CN" of PAN, while which at 1740 cm^{-1} may be caused by the "−C═O" of DMF, the solvent of PAN. The absorption peaks at 2921 and 1240 cm^{-1} are attributed to the stretching vibrations of "−CH".

The specific surface areas and pore sizes of the hierarchical nanofiber membranes were determined by the nitrogen adsorption−desorption measurement (Figure 3d). The obtained isotherm of PAN, Fe_3O_4@PAN, and Fe_3O_4@PAN/CS nanofiber membranes followed IUPAC type IV structure, indicating the typically mesoporous structure. Instead, the composite membranes displayed type H_4 hysteresis loop at the relative pressure ranging from 0.35 to 0.95 nm, further confirming the existence of mesoporous and multilayer packing structure. The surface area calculated from the BET method of Fe_3O_4@PAN/CS composite membranes was 20.412 $m^2\ g^{-1}$, which is larger than that of the raw PAN membrane (15.912 $m^2\ g^{-1}$). The corresponding pore size distributions of the membrane are presented in Figure 4a. The average pore sizes of Fe_3O_4@PAN/CS and PAN nanofiber membranes are 20.128 and 26.343 nm, respectively. The combination of

https://dx.doi.org/10.1021/acsapm.0c00988
ACS Appl. Polym. Mater. 2020, 2, 5686−5697

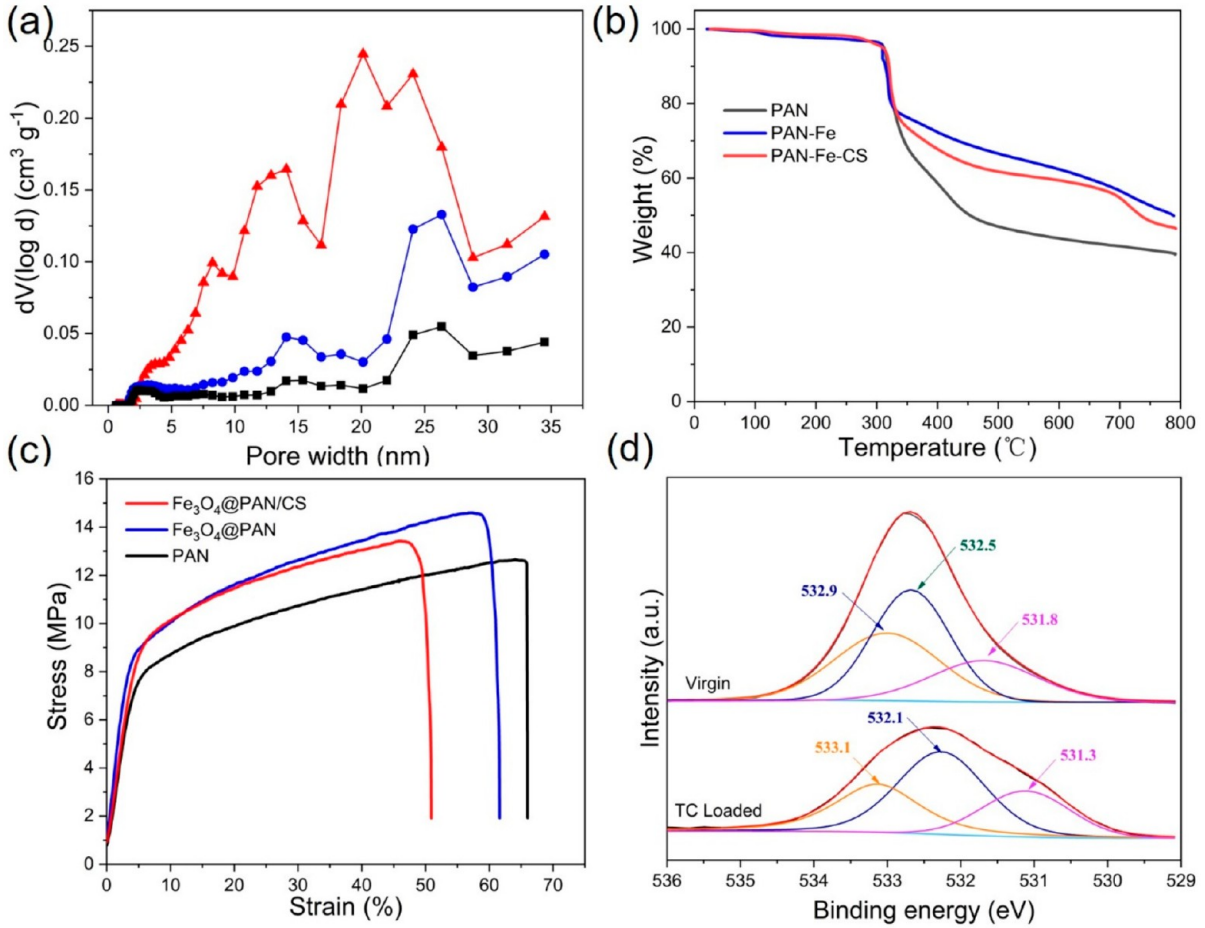

Figure 4. Characterization of the gas-spinning membranes: (a) pore size distribution, (b) thermogravimetric curve, and (c) stress−strain curve of PAN, Fe_3O_4@PAN, and Fe_3O_4@OAN/CS membranes. (d) O 1s XPS spectra of the Fe_3O_4@PAN/CS composite membrane.

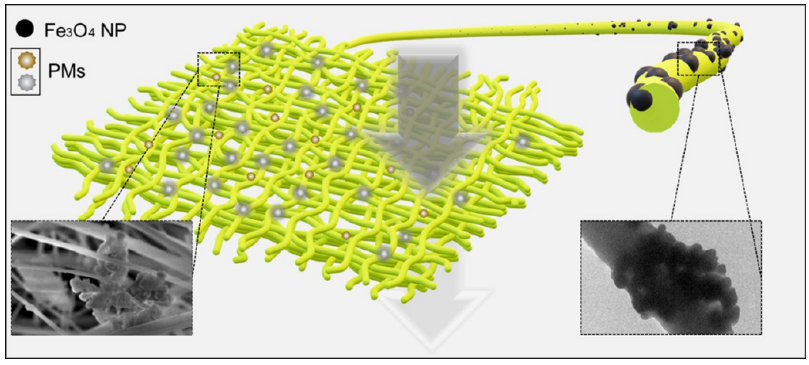

Figure 5. Proposed PMs filtration mechanism of the Fe_3O_4@PAN/CS. Inset is the SEM image of the surface of the Fe_3O_4@PAN/CS (left) and the TEM image of the composite nanofibers (right).

agglomerate Fe_3O_4 nanoparticles and interlaced PAN nanofibers allows the formation of a 3D porous network architecture, which will be helpful for the efficient removal of harmful substrates.

As shown in Figure 4b, the membrane shows little change in weight before 300 °C. With the increasing of temperature, the Fe_3O_4@PAN/CS nanofibrous membrane degraded, followed by a fast weight decrease at higher temperature. Finally, the weight percentage decreased slowly and tended to be stabilized after 500 °C. The thermal stability of these membranes increased after the incorporation of Fe_3O_4 NPs.

Considering that the mechanical strength of the Fe_3O_4@PAN/CS composite fiber membranes would directly affect the application performance and service life when applied in practical applications. The mechanical performance of the composite membranes was measured and presented in Figure 4c. Results turned out that the tensile strength of the membrane increased from 12.6 to 14.6 MPa after the incorporation of Fe_3O_4 NPs, while the membrane strain decreased from 64% to 51% when covered by CS coating. The incorporation of Fe_3O_4 NPs could significantly enhance the mechanical strength of the membranes. The leaching test (Supporting Information) was performed to evaluate the

https://dx.doi.org/10.1021/acsapm.0c00988
ACS Appl. Polym. Mater. 2020, 2, 5686−5697

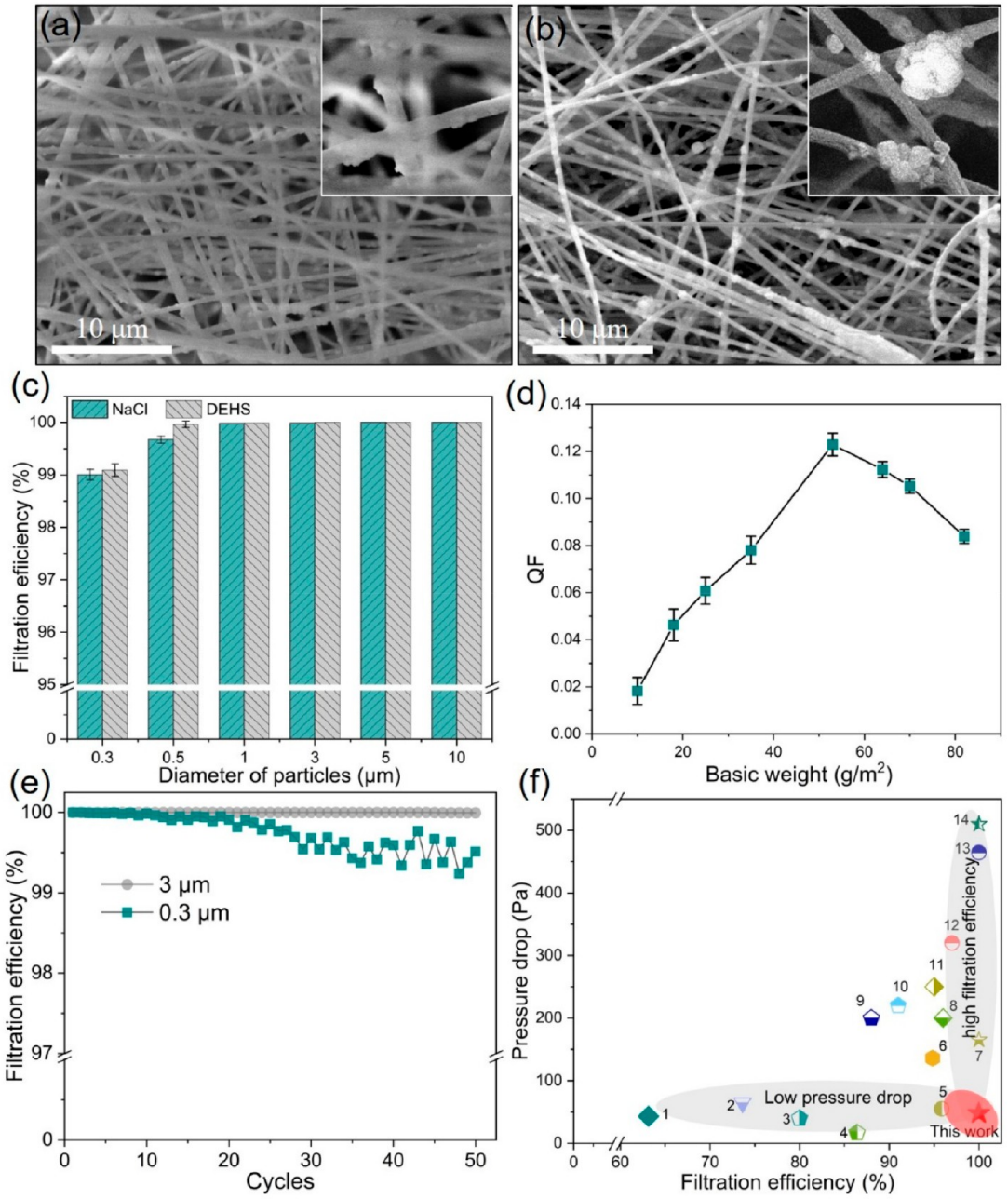

Figure 6. Air filtration performance of the Fe_3O_4@PAN/CS nanofiber membranes. SEM images of the nanofiber membrane (a) before and (b) after the air filtration process; the scale bar of the inset images was 1 μm. (c) Air filtration efficiency of the membranes varying in PMs diameters. (d) QF value of the membranes of different basic weights. (e) Air filtration efficiency of the membranes after 50 cycles. (f) Comparison of this work and previous works; references are provided in Table S2.

stability of the adsorbent. The result showed that the concentrations of Fe were <0.005−32.180 μg L^{-1} between 0 and 48 h (Table S1), far lower than the accepted concentration of Fe_3O_4 (as Fe) suggested by the WHO Guidelines for Drinking-water Quality (2 mg L^{-1}, which does not present a hazard to health). The obtained results indicate that the attachments between the Fe_3O_4 NPs and nanofibers are strong, and the Fe_3O_4@PAN/CS composite membrane do not pose any danger for drinking water treatment since the leached metal concentrations were far below the maximum allowable concentrations.

3.2. Air Filtration Performances of Fe_3O_4@PAN/CS Composite Nanofibrous Membrane. As illustrated in Figure 5, Fe_3O_4 NPs were blended in the PAN nanofiber, which could increase the specific surface area of the filter membrane, on the one hand, and provide more active sites on the other. The filtration performance of the Fe_3O_4@PAN/CS composite membrane was investigated in Figure 6. The filtration efficiency and pressure drop of the membrane varying in particulates ranging from 300 nm to 10 μm were investigated, and the air flow was set to be 85 L min^{-1} (Figure 6c). Additionally, compared to the membrane without Fe_3O_4 nanoparticles, the membranes with different Fe_3O_4 dosages show higher filtration efficiency (Figure S5); the higher the loaded content of Fe_3O_4, the higher the filtration efficiency. Our proposal further confirmed that the Fe_3O_4 NPs

https://dx.doi.org/10.1021/acsapm.0c00988
ACS Appl. Polym. Mater. 2020, 2, 5686−5697

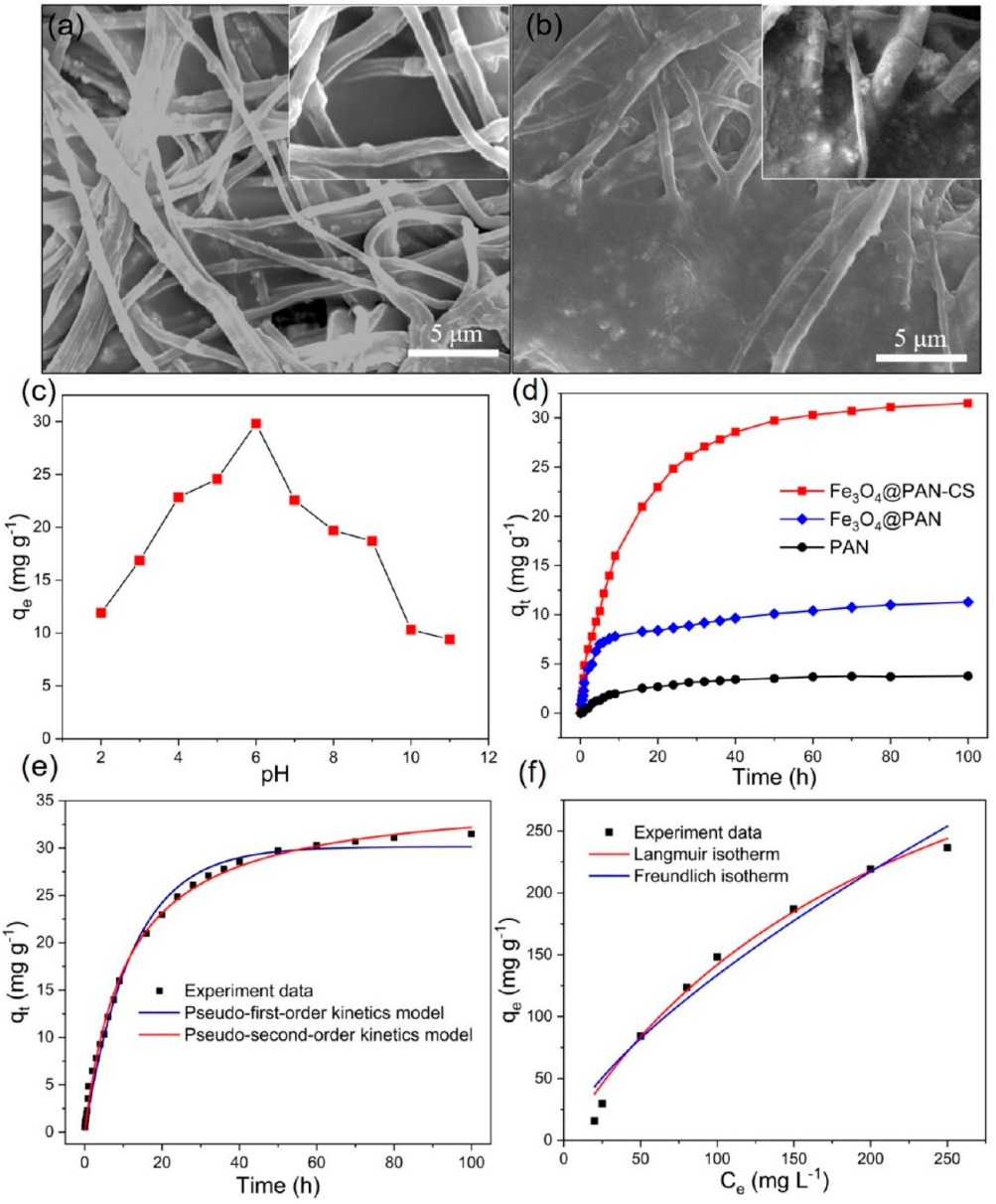

Figure 7. TC adsorption performance of the Fe_3O_4@PAN/CS membrane. SEM images show the surface morphology of the membrane (a) before and (b) after TC adsorption; the scale bar of the inset images was 1 μm. (c) Adsorption capacities of the PAN, Fe_3O_4@PAN, and Fe_3O_4@PAN/CS membrane. (d) Equilibrium adsorbing quantity of TC on Fe_3O_4@PAN/CS membrane varying in solution pH. (e) Adsorption kinetics and (f) adsorption isotherm of TC on Fe_3O_4@PAN/CS composite membrane.

could provide more active sites for the robust interaction between the filter membrane and particulates. The typical SEM morphologies of the Fe_3O_4@PAN/CS composite membranes after the air filtration process are presented in Figure 6a,b. The SEM images shown in Figure 6b indicated that besides the loaded Fe_3O_4 NPs, all the particles attached to the fibers were the ultrathin particles captured by the filter during the air filtration test. The large particles can be directly intercepted by the filter and accumulated on the surface of the membrane, and the ultrathin particles will go through into the inter channels of the nanofiber membrane, finally adhered to the fibers. The general hierarchical architecture will not be affected; thus, the membrane could maintain long-term filtration performance.

The filtration efficiency of the composite Fe_3O_4@PAN/CS membranes for both PMs with diameters of 300 nm were respectively 99.01% and 99.09%, while it was 99.67% and 99.96% for the oil and non-oil PMs of 500 nm (Figure 6c). It is interesting that the filtration efficiency almost approaching to 100% when the PMs are larger than 1 μm (e.g., 1, 3, 5, and 10 μm), while the commercial filters usually show relative lower filtration efficiency; details are provided in the Supporting Information. The filtration efficiency for both oil and non-oil types PMs tend to improve after the addition of Fe_3O_4 NPs, since the surface roughness and specific surface area increased. The strategy of incorporating nanoparticles to enhance the interaction of composite membrane and PMs is proved to be effective. Pore size characterization from the BET method showed that the average pore size was 22.356 nm, which is smaller than the particles, further confirming the interception function of the membrane. Additionally, at the comparable

https://dx.doi.org/10.1021/acsapm.0c00988
ACS Appl. Polym. Mater. 2020, 2, 5686−5697

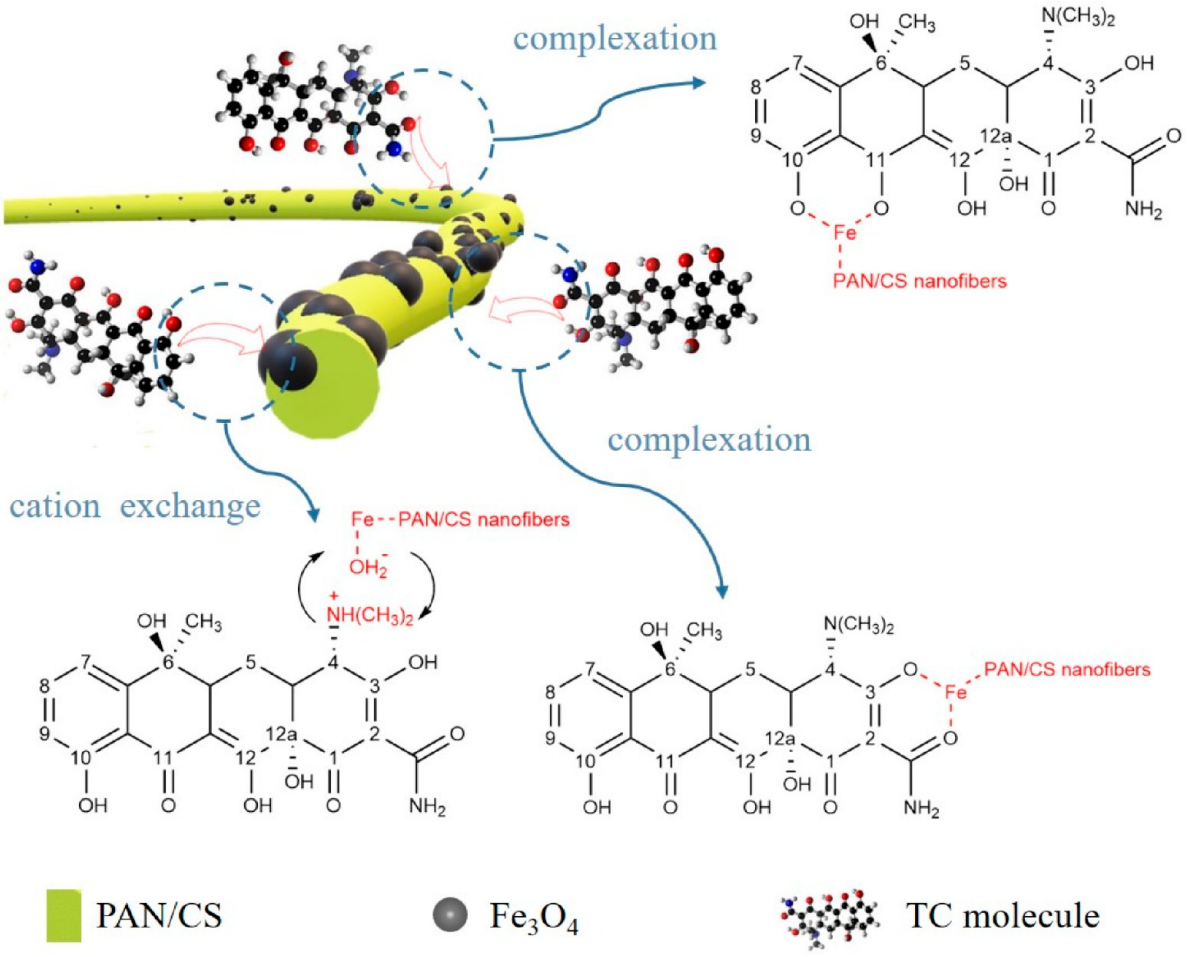

Figure 8. Illustration of the adsorption of TC on Fe_3O_4@PAN/CS composite nanofibers. Note: these schematics are not drawn to scale.

filtration efficiency of about 99.9%, the pressure drop of the composite membrane generated by the gas-spinning method is only 48 Pa, which is far lower than 510 Pa reported by the previously reported filter media (Figure 6f and Table S2), further showing the superiority of the composite membranes prepared by the gas-spinning technology.

We further investigated the air filtration performance varying in basic weight and air flow. Results turned out that increased membrane basic weight results in increased air filtration performance (Figure S6a). Additionally, with the increasing of air flow, the membrane shows lower filtration performance: the filtration efficiency decreased, and the pressure drop increased (Figure S6b). Considering the tread-off relationship between filtration efficiency and pressure drop, the QF value was induced to evaluate the air filtration performance more directly. The larger the QF value, the more superior the air filtration performance. As shown in Figure 6d, the QF value (0.123) of the membrane (basic weight 53 g m^{-2}) was found to be larger than that of the other groups, which means the membrane possessed a low pressure drop and a relatively high removal efficiency.

The air filtration tests were repeated 50 cycles to evaluate the reusability and durability and the feasibility of large-scale application of the Fe_3O_4@PAN/CS composite membrane. As shown in Figure 6e, even after 30 cycles of continuous use, the filtration efficiency of Fe_3O_4@PAN/CS composite fiber membrane could maintain more than 99.5% for ultrathin PMs with a diameter of 300 nm. The composite fiber membrane can still maintain 99.99% filtration efficiency for PMs of 3 μm (almost 100% for PMs of 5 and 10 μm) even after 50 cycles of recycling. Obviously, the Fe_3O_4@PAN/CS composite air filtration membrane shows excellent durability and can be reused many times.

3.3. Antibiotic Adsorption Performance Study. The antibiotic adsorption performance of the membrane was studied and presented in Figure 7. The preliminary research about the TC adsorption performance for a series of PAN-based nanofibers was carried out; the results indicated that the composite Fe_3O_4@PAN/CS composite membrane can effectively adsorb TC while the pure PAN membrane almost showed no TC adsorption (Figure 7c). The adsorption capacity of the Fe_3O_4@PAN/CS composite membrane for TC is 31.49 ± 0.43 mg g^{-1}, which is much higher than that of the Fe_3O_4@PAN blended membrane (11.28 ± 0.23 mg g^{-1}) and the pure PAN nanofiber membrane (3.47 ± 0.16 mg g^{-1}). The adsorption capacity increased obviously with the increasing of Fe_3O_4 content (Figure S7). The superiority of the composite membrane may attribute to the formation of stable metal−ligand complex between Fe_3O_4 and TC compounds;[32] in addition, the large amount of free amino groups and hydroxyl groups on the framework of chitosan make it easy to interact with the carboxyl groups, keto groups, and amino groups of the antibiotics, thus realizing the adsorption of TC.[33]

https://dx.doi.org/10.1021/acsapm.0c00988
ACS Appl. Polym. Mater. 2020, 2, 5686−5697

Considering the surface properties of the Fe_3O_4@PAN/CS composite nanofibrous membrane, such as the amount of hydroxyl moieties, the charges on the membrane surface, etc., would be affected by the solution pH. Here, the TC adsorption behavior of the Fe_3O_4@PAN/CS nanofiber membrane varying in different pH condition was investigated. The pK_{a1}, pK_{a2}, and pK_{a3} value of TC are 3.30, 7.68, and 9.68.[28] The adsorption capacity of the composite membrane varying in solution pH was determined. The adsorption capacity increases tremendously with the solution pH increasing from 2 while decreases with the solution pH further increasing from 6 to 1; when the pH was around 6, the highest adsorption capacity (30.03 ± 0.57 mg g^{-1}) was studied (Figure 7c). The possible explanation could be when the solution pH is below 6. The electrostatic repulsion formed since the adsorbent was positively charged, and the dominant specie of TC was TCH_3^+; thus, the adsorption performance was affected. Similarly, when the pH increased to above 6, the dominant species of TC became TCH^- and TC^{2-}, which could also form electrostatic repulsion with the negatively charged adsorbent. The stronger electrostatic repulsion results in reduced adsorption affinity of TC to the adsorbent, finally leading to the reduced adsorption capacity. When the solution pH is around 6, TCH_2 is the dominant species of TC, and the adsorbent is neutrally charged, the electrostatic repulsion between which is lowest; thus, the adsorption capacity tends to be highest at pH around 6.[28]

The XPS spectrum of the membrane was analyzed to study the adsorption behavior more deeply, as shown in Figure 4d. The peak appeared at 531 eV is ascribed to the lattice oxygen in the metal oxide (Fe−O), and the peak located at 532.5 eV may due to the surface H−O hydroxyl group, and which appeared at 532.9 eV is attributed to the single C−O bonds. The increase of the relative content of "Fe−O" bond after TC adsorption confirmed that the adsorption mechanism was mainly attributed to the substitution of "Fe−OH" groups. Meanwhile, the proportion of the "H−O" decreased significantly, indicating the exchange between the surface hydroxyl groups and TC molecules. The adsorption process was mainly demonstrated through way of cation exchange and complex formation, as illustrated in Figure 8.

The TC adsorption capacity increased rapidly in the first 20 h and then increased slowly; the adsorption equilibrium was obtained after 80 h (Figure 7d). We further investigate the TC adsorption kinetics by the commonly used pseudo-first-order and pseudo-second-order kinetics models; the detailed formulas are respectively given by eqs 5 and 6 in the Supporting Information. As shown in Table S3 and Figure 7e, the pseudo-second-order model (R^2 > 0.996) can better fit the experimental adsorption kinetics data, which means the TC adsorption process was dominated by chemisorption, confirming our hypothesis that the surface complexation happened during the adsorption process.

The adsorption isotherm experiment varying in TC concentrations (10−250 mg L^{-1}) was performed to determine the maximum adsorption capacity and the surface properties of the Fe_3O_4@PAN/CS nanofiber membrane (Figure 7f). Both the Langmuir isotherm model and the Freundlich isotherm model were applied to analyze the adsorption process; detailed formulas are presented in eqs 7 and 8 of the Supporting information. As shown in Table S4 and Figure 7f, the Langmuir isotherm (R^2 > 0.997) can better fit the experimental data, indicating the single-layer adsorption of TC on the membrane surfaces.

The chitosan coating at the surface of the composite membrane and the loaded Fe_3O_4 NPs (5 wt %) are beneficial for the removal of TC. The maximum adsorption capacity was calculated to be 468.33 mg g^{-1}, which is higher than those for the Fe_3O_4 NPs reported in a previous study (Table S5). The comparison work between the Fe_3O_4@PAN/CS composite membrane and other previously reported adsorbents is presented in Table S5; the results indicate that our designed hierarchical composite membrane could achieve higher or comparable adsorption performance.

The adsorption−desorption experiments were performed to determine the reusability and durability of the composite membrane. Here, a 0.1 M NaOH solution was chosen as the regenerative desorbent and repeated five times for adsorption−desorption. The morphologies of the composite membrane before and after the adsorption cycles are provided in Figure 7a,b; the surface structure was almost maintained, and there is no obvious damage, indicating the stability of the composite membrane. In addition, the EDS spectrum and EDS mappings of the composite membrane after multiple uses are provided in Figure S8; both Na and Cl were founded, which may be attributed to the NaOH and tetracycline hydrochloride. As shown in Figure 9, the adsorption efficiency of the regenerated

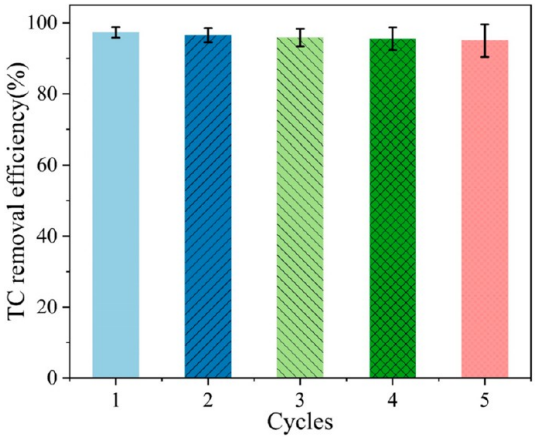

Figure 9. Regeneration and reusability of the Fe_3O_4@PAN/CS composite membrane for TC removal over five adsorption−desorption cycles.

Fe_3O_4@PAN/CS membrane could maintain 95% even after five adsorption−desorption cycles, which only decreased 1−2% compared to the original adsorption efficiency, demonstrating the reusability and stability. The high porosity and interconnected pore channel structure of the gas-spinning nanofiber membranes reduce the possible block of membrane pores and make the NaOH solution contact with the adsorbed TC closely, thus achieving a good regeneration ability.

3.4. Oil−Water Separation Performance. The surface wetting property of the Fe_3O_4@PAN/CS nanofiber membranes was studied by a contact angle analyzer. As shown in Figure S9a, the oil (*n*-hexane) droplet could easily move and leave the membrane surface without any residue even under pressure, demonstrating the superoleophobicity of oil in air. In addition, the underwater oil contact angle (OCA) varying in Fe_3O_4 content was investigated; the OCA increased obviously with the increase of Fe_3O_4 content (Figure S10). It is

https://dx.doi.org/10.1021/acsapm.0c00988
ACS Appl. Polym. Mater. 2020, 2, 5686−5697

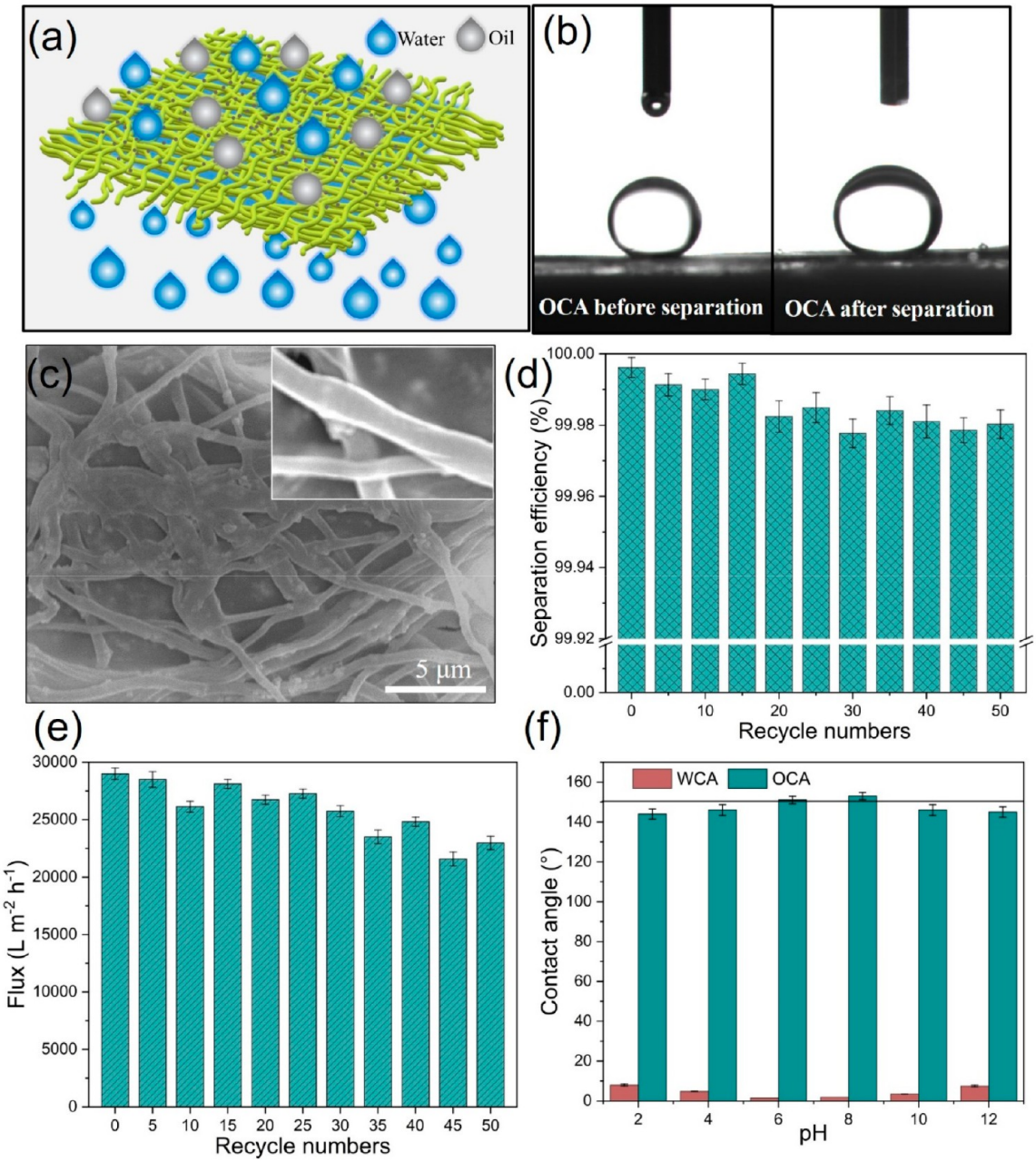

Figure 10. Regeneration and reusability of the Fe_3O_4@PAN/CS composite membrane. (a) Illustration of the proposed oil−water separation mechanism. (b) Surface wettability of the membrane before and after 50 reuse cycles; the oil contact angle in air was investigated. (c) SEM images of the membrane surface. (d) Separation efficiency and (e) penetration flux of the Fe_3O_4@PAN/CS composite membrane over 50 cycles. (f) Water and oil contact angles of the Fe_3O_4@PAN/CS composite membrane after immersing in strong acidic and alkaline aqueous solution.

noteworthy that the water droplet wetted and immersed in the surface of the membrane at extremely fast speed (within 0.4 s) (Figure S9b). Additionally, the water contact angle (WCA) of the designed composite membrane in air was nearly 0°, indicating the superhydrophilicity performance of the multifunctional membrane. As mentioned above, the composite membrane exhibited great potential in water treatment. Here, as shown in Figure 10, the Fe_3O_4@PAN/CS composite membrane with superhydrophobic and superoleophilic properties is applied in oily water separation.

The oil−water separation process is illustrated in Figure 10a, the setup for which is presented in Figure S9c. The details of the separation process are provided in the Supporting Information. As record by the camera, the composite membrane separated 20 mL of the oil and water mixture within just 7.21 s, demonstrating the ultrahigh separation flux and good separation performance. Additionally, no visible oil droplets can be observed in the collected water after separation process, indicating a high separation efficiency of the Fe_3O_4@PAN/CS membrane.

By virtue of the superior superhydrophilicity, the permeation flux of the designed membrane was more than 28996 ± 216 L m^{-2} h^{-1}, much higher than most of the previous related work which are within 9000 L m^{-2} h^{-1} (Table S6). It is really hard to achieve such an ultrahigh throughput of 28996 ± 216 L m^{-2} h^{-1} without any extra pressure and just under gravity. In

https://dx.doi.org/10.1021/acsapm.0c00988
ACS Appl. Polym. Mater. 2020, 2, 5686−5697

addition, the oily water separation efficiency of the membrane was determined to be more than 99.99%. The superior separation performance of the multifunctional Fe_3O_4@PAN/CS membrane was attributed to the hierarchical 3D network architecture and the superhydrophilicity and superoleophobicity of the material itself.

The reusability of the Fe_3O_4@PAN/CS membrane for oil−water separation was characterized to further evaluate the potential practical application. The regeneration tests were performed by washing the composite membrane with ethanol after every separation process and then dried and used for the next cycle. The wettability and surface morphology of the membrane after 50 cycles are characterized and presented in Figure 10b,c; the wetting properties were maintained well even after 50 reuse cycles, and the channel structure of the fibers was slightly blocked, which may result in compromised separation performance. The separation fluxes and efficiency were relatively stable, as shown in Figure 10d,e. In detail, the Fe_3O_4@PAN/CS composite membrane maintained more than 99.9% separation efficiency even after 50 cycles without the compromise of permeation flux which could keep of more than 22979 L m^{-2} h^{-1}. The comparison between the Fe_3O_4@PAN/CS composite membrane and other previously reported separation membrane is presented in Table S6. The composite membrane could achieve higher or comparable oil−water separation efficiency and flux, demonstrating the superiority as well as the efficient separation performance of the designed blend structure. With the increase of the cycles, there is a slight decrease in both oil−water separation efficiency and separation flux, which may due to the blocked pores of the hierarchical structure of the membrane.

We further investigated the chemical environmental durability of the oil−water separation membrane in harsh conditions. The membrane was immersed in solutions of various pH (2−12) to evaluate the surface wetting properties; as shown in Figure 10f, the membrane still maintained high superhydrophilicity and superoleophobicity after immersing in both acidic and alkaline aqueous solution, indicating the versatility and stability of the multifunctional Fe_3O_4@PAN/CS composite membrane.

CONCLUSION

In summary, the gas-spinning strategy is proposed to generate ultrathin nanofiber membranes with high porosity and interconnected channeling pore structures in a simple, green, and scalable way. The multifunctional Fe_3O_4@PAN/CS composite nanofiber membrane not only shows high efficient removal of PMs in the air but also possesses great potential in antibiotic adsorption and oil−water separation. The air filtration efficiency is more than 99.98% for 300 nm ultrathin particles, which is approaching 100% for particles larger than 1 μm, and the pressure drop is only 48 Pa. The 3D network structure allows robust and comparatively high adsorption performance for TC; the maximum adsorption capacity (Langmuir isotherm) is 468.33 mg g^{-1} at the equilibrium pH of 6. In addition, the composite membrane possesses more than 99.9% separation efficiency for oil−water mixture at the permeation flux of about 28996 L m^{-2} h^{-1}. Moreover, the reusability and durability of the multifunctional Fe_3O_4@PAN/CS membrane for the highly efficient applications in air filtration, antibiotic removal, and oil−water separation were investigated, demonstrating the potential long-term scaled-up applications.

ASSOCIATED CONTENT

Supporting Information

The Supporting Information is available free of charge at https://pubs.acs.org/doi/10.1021/acsapm.0c00988.

Air filtration, antibiotic adsorption, oil−water separation, gas-spinning setup, air filtration measurement, leaching test, SEM images, EDS spectrum, EDS mapping images, comparison of filtration performance, TC chemical structure, TC adsorption capacity, TC adsorption parameters, comparison of TC adsorption, underwater oil contact angle, comparison of oil−water separation performance, and related references (PDF)

AUTHOR INFORMATION

Corresponding Authors

Chaobo Huang − *Joint Laboratory of Advanced Biomedical Technology (NFU-UGent), College of Chemical Engineering, Nanjing Forestry University (NFU), Nanjing 210037, P. R. China; Laboratory of Biopolymer based Functional Materials, Nanjing Forestry University, Nanjing 210037, P. R. China;* orcid.org/0000-0003-3484-0545; Email: huangchaobo@njfu.edu.cn

Ranhua Xiong − *Lab General Biochemistry & Physical Pharmacy, Department of Pharmaceutics, Ghent University, Ghent 9000, Belgium*; Email: ranhua.xiong@gmail.com

Authors

Dan Lv − *Joint Laboratory of Advanced Biomedical Technology (NFU-UGent), College of Chemical Engineering, Nanjing Forestry University (NFU), Nanjing 210037, P. R. China*

Guosheng Tang − *Joint Laboratory of Advanced Biomedical Technology (NFU-UGent), College of Chemical Engineering, Nanjing Forestry University (NFU), Nanjing 210037, P. R. China*

Long Chen − *Joint Laboratory of Advanced Biomedical Technology (NFU-UGent), College of Chemical Engineering, Nanjing Forestry University (NFU), Nanjing 210037, P. R. China*

Mengjie Zhang − *Joint Laboratory of Advanced Biomedical Technology (NFU-UGent), College of Chemical Engineering, Nanjing Forestry University (NFU), Nanjing 210037, P. R. China*

Jiaxin Cui − *Joint Laboratory of Advanced Biomedical Technology (NFU-UGent), College of Chemical Engineering, Nanjing Forestry University (NFU), Nanjing 210037, P. R. China*

Complete contact information is available at: https://pubs.acs.org/10.1021/acsapm.0c00988

Author Contributions

D.L. and G.T. contributed equally to this work.

Notes

The authors declare no competing financial interest.

ACKNOWLEDGMENTS

The National Natural Science Foundation of China (Nos. 21774060 and 31770609), the National Key R&D Program of China (2017YFF0207800), the Jiangsu key lab of biomass-based energy and Materials (JSBEM2016011), and the Natural Science Key Project of the Jiangsu Higher Education Institutions (16KJA220006) are acknowledged with gratitude.

https://dx.doi.org/10.1021/acsapm.0c00988
ACS Appl. Polym. Mater. 2020, 2, 5686−5697

REFERENCES

(1) Shannon, M. A.; Bohn, P. W.; Elimelech, M.; Georgiadis, J. G.; Marinas, B. J.; Mayes, A. M. Science and technology for water purification in the coming decades. *Nature* **2008**, *452*, 301−310.

(2) Bolisetty, S.; Reinhold, N.; Zeder, C.; Orozco, M. N.; Mezzenga, R. Efficient purification of arsenic-contaminated water using amyloid−carbon hybrid membranes. *Chem. Commun.* **2017**, *53*, 5714−5717.

(3) Kota, A. K.; Kwon, G.; Choi, W.; Mabry, J. M.; Tuteja, A. Hygro-responsive membranes for effective oil−water separation. *Nat. Commun.* **2012**, *3*, 1−8.

(4) Gao, X.; Zhou, J.; Du, R.; Xie, Z.; Deng, S.; Liu, R.; Liu, Z.; Zhang, J. Robust Superhydrophobic Foam: A Graphdiyne-Based Hierarchical Architecture for Oil/Water Separation. *Adv. Mater.* **2016**, *28*, 168−173.

(5) Zhang, Q.; Jiang, X.; Tong, D.; Davis, S. J.; Zhao, H.; Geng, G.; Feng, T.; Zheng, B.; Lu, Z.; Streets, D. G.; Ni, R.; Brauer, M.; van Donkelaar, A.; Martin, R. V.; Huo, H.; Liu, Z.; Pan, D.; Kan, H.; Yan, Y.; Lin, J.; He, K.; Guan, D. Transboundary health impacts of transported global air pollution and international trade. *Nature* **2017**, *543*, 705−709.

(6) Lelieveld, J.; Evans, J. S.; Fnais, M.; Giannadaki, D.; Pozzer, A. The contribution of outdoor air pollution sources to premature mortality on a global scale. *Nature* **2015**, *525*, 367−371.

(7) Zhang, R.; Liu, C.; Hsu, P. C.; Zhang, C.; Liu, N.; Zhang, J.; Lee, H. R.; Lu, Y.; Qiu, Y.; Chu, S.; Cui, Y. Nanofiber Air Filters with High-Temperature Stability for Efficient PM2.5 Removal from the Pollution Sources. *Nano Lett.* **2016**, *16*, 3642−3649.

(8) Yousefi, N.; Lu, X.; Elimelech, M.; Tufenkji, N. Environmental performance of graphene-based 3D macrostructures. *Nat. Nanotechnol.* **2019**, *14*, 107−119.

(9) Sun, H.; Zhu, J.; Baumann, D.; Peng, L.; Xu, Y.; Shakir, I.; Huang, Y.; Duan, X. Hierarchical 3D electrodes for electrochemical energy storage. *Nat. Rev. Mater.* **2019**, *4*, 45−60.

(10) Wu, C.; Zeng, X.; He, P.; Chen, L.; Wei, W. Flexible WS_2@CNFs membrane electrode with outstanding lithium storage performance derived from capacitive behavior. *Adv. Mater. Interfaces* **2018**, *5*, 1701080.

(11) Yoon, J.; Yang, H. S.; Lee, B. S.; Yu, W. R. Recent progress in coaxial electrospinning: new parameters, various structures, and wide applications. *Adv. Mater.* **2018**, *30*, 1704765.

(12) Wang, Z.; Liu, X.; Macosko, C. W.; Bates, F. S. Nanofibers from water-extractable melt-blown immiscible polymer blends. *Polymer* **2016**, *101*, 269−273.

(13) Badrossama y, M. R.; McIlwee, H. A.; Goss, J. A.; Parker, K. K. Nanofiber Assembly by Rotary Jet-Spinning. *Nano Lett.* **2010**, *10*, 2257−2261.

(14) Tang, G.; Xiong, R.; Lv, D.; Xu, R. X.; Braeckmans, K.; Huang, C.; De Smedt, S. C. Gas−Shearing Fabrication of Multicompartmental Microspheres: A One−Step and Oil−Free Approach. *Adv. Sci.* **2019**, *6*, 1802342.

(15) Daristotle, J. L.; Behrens, A. M.; Sandle r, A. D.; Kofinas, P. A review of the fundamental principles and applications of solution blow spinning. *ACS Appl. Mater. Interfaces* **2016**, *8*, 34951−34963.

(16) Yuan, Y.; Zhao, S.; Wen, J.; Wang, D.; Guo, X.; Xu, L.; Wang, X.; Wang, N. Rational Design of Porous Nanofiber Adsorbent by Blow−Spinning with Ultrahigh Uranium Recovery Capacity from Seawater. *Adv. Funct. Mater.* **2019**, *29*, 1805380.

(17) Lv, D.; Zhu, M.; Jiang, Z.; Jiang, S.; Zhang, Q.; Xiong, R.; Huang, C. Green electrospun nanofibers and their application in air filtration. *Macromol. Mater. Eng.* **2018**, *303*, 1800336.

(18) Liu, L.; Liu, Z.; Bai, H.; Sun, D. D. Concurrent filtration and solar photocatalytic disinfection/degradation using high-performance Ag/TiO_2 nanofiber membrane. *Water Res.* **2012**, *46*, 1101−1112.

(19) Zhang, Y. Q.; Yang, X. B.; Wang, Z. X.; Long, J.; Shao, L. Designing multifunctional 3D magnetic foam for effective insoluble oil separation and rapid selective dye removal for use in wastewater remediation. *J. Mater. Chem. A* **2017**, *5*, 7316−7325.

(20) Esmaeili, A.; Beni, A. A. Optimization and design of a continuous biosorption process using brown algae and chitosan/PVA nano-fiber membrane for removal of nickel by a new biosorbent. *Int. J. Environ. Sci. Technol.* **2018**, *15*, 765−778.

(21) Chu, Z.; Feng, Y.; Seeger, S. Oil/water separation with selective superantiwetting/superwetting surface materials, Angew. *Angew. Chem., Int. Ed.* **2015**, *54*, 2328−2338.

(22) Wen, G.; Gao, X.; Guo, Z. Simple fabrication of a multifunctional inorganic paper with high efficiency separations for both liquids and particles. *J. Mater. Chem. A* **2018**, *6*, 21524−21531.

(23) Lv, D.; Wang, R.; Tang, G.; Mou, Z.; Lei, J.; Han, J.; De Smedt, S.; Xiong, R.; Huang, C. Ecofriendly electrospun membranes loaded with visible-light-responding nanoparticles for multifunctional usages: highly efficient air filtration, dye scavenging, and bactericidal activity. *ACS Appl. Mater. Interfaces* **2019**, *11*, 12880−12889.

(24) Navrotsky, A.; Mazeina, L.; Majzlan, J. Size-Driven Structural and Thermodynamic Complexity in Iron Oxides. *Science* **2008**, *319*, 1635.

(25) Xu, P.; Zeng, G. M.; Huang, D. L.; Feng, C. L.; Hu, S.; Zhao, M. H.; Lai, C.; Wei, Z.; Huang, C.; Xie, G. X.; Liu, Z. F. Use of iron oxide nanomaterials in wastewater treatment: A review. *Sci. Total Environ.* **2012**, *424*, 1−10.

(26) Bae, J.; Baek, I.; Choi, H. Mechanically enhanced PES electrospun nanofiber membranes (ENMs) for microfiltration: The effects of ENM properties on membrane performance. *Water Res.* **2016**, *105*, 406−412.

(27) Ye, H.; Zhu, L.; Li, W.; Liu, H.; Chen, H. Constructing fluorine-free and cost-effective superhydrophobic surface with normal-alcohol-modified hydrophobic SiO_2 nanoparticles. *ACS Appl. Mater. Interfaces* **2017**, *9*, 858−867.

(28) Liu, Q.; Zhong, L. B.; Zhao, Q. B.; Frear, C.; Zheng, Y. M. Synthesis of Fe_3O_4/polyacrylonitrile composite electrospun nanofiber mat for effective adsorption of tetracycline. *ACS Appl. Mater. Interfaces* **2015**, *7*, 14573−14583.

(29) Zhou, Z.; La i, C.; Zhang, L.; Qian, Y.; Hou, H.; Reneker, D. H.; Fong, H. Development of carbon nanofibers from aligned electrospun polyacrylonitrile nanofiber bundles and characterization of their microstructural, electrical, and mechanical properties. *Polymer* **2009**, *50*, 2999−3006.

(30) Xiao, L.; Li, J.; Brougham, D. F.; Fox, E. K.; Feliu, N.; Bushmelev, A.; Schmidt, A.; Mertens, N.; Kiessling, F.; Valldor, M.; Fadeel, B.; Mathur, S. Water-soluble superparamagnetic magnetite nanoparticles with biocompatible coating for enhanced magnetic resonance imaging. *ACS Nano* **2011**, *5*, 6315−6324.

(31) Cho, W.; Park, S.; Oh, M. Coordination polymer nanorods of Fe-MIL-88B and their utilization for selective preparation of hematite and magnetite nanorods. *Chem. Commun.* **2011**, *47*, 4138−4140.

(32) Xiong, W.; Zeng, Z.; Zeng, G.; Yang, Z.; Xiao, R.; Li, X.; Cao, J.; Zhou, C.; Chen, H.; Jia, M.; Yang, Y.; Wang, W.; Tang, X. Metal-organic frameworks derived magnetic carbon-αFe/Fe_3C composites as a highly effective adsorbent for tetracycline removal from aqueous solution. *Chem. Eng. J.* **2019**, *374*, 91−99.

(33) Zhang, S.; Dong, Y.; Yang, Z.; Yang, W.; Wu, J.; Dong, C. Adsorption of pharmaceuticals on chitosan-based magnetic composite particles with core-brush topology. *Chem. Eng. J.* **2016**, *304*, 325−334.

https://dx.doi.org/10.1021/acsapm.0c00988
ACS Appl. Polym. Mater. 2020, 2, 5686−5697